Developing Geothermal Energy from Hydrothermal and EGS Sources while Minimizing Risks and hazards

Bazargan Mohsen[1,2], Gudmundsson Agust[1], Meredith Philip[2], Kenyon Isaac[1].

[1] Royal Holloway University of London, Earthscience department, Egham, Surrey, UK

[2] University College London, Earthscience department, London, London, UK

Mohsen.Bazargan.2014@live.rhul.ac.uk

Keywords: crack propagation; extended finite element method; fracture mechanics; Hydraulic fracturing; pre-existing faults

ABSTRACT

Deep geothermal energy is increasingly being explored as an attractive alternative energy source. This research uses field data and analysis in combination with experimental tests and numerical/analytical models for understanding better induced fracturing of geothermal and shale-gas reservoirs. The rock-physics tests carried out in this project use different boundary conditions so as to verify the results of the analytical investigation and numerical simulations. Also, sills are common in the sedimentary basins worldwide and, through thermal effects, may change organic material into oil and gas. Many thick sills worldwide are currently exploited as hydrocarbon reservoirs and the Bight Basin is one of them. Another aim of this study is to use numerically based modeling on the linear elasticity theory a seismic section of the Bight Basin, S. Australia to understand the relationship of sill emplacement in a heterogeneous rock body of deltaic and marine stratigraphy. As well as to understand the relation of this emplacement to fracture reactivation potential through interconnected fracture cluster accumulations.

1. INTRODUCTION

The aim of this research is to provide new methods and techniques that can contribute to the development and optimization of the geothermal energy, with application to Europe. Geothermal energy is a renewable source of energy that can provide constant power and heat. The technologies to exploit this potential are commercially available today. In Europe, the geologic or theoretical potential is very large and exceeds current electricity demand in some countries. However, distribution of geothermal heat is highly variable and only a small part of the theoretical potential can actually be exploited, because of technical and economic barriers. Here we provide an overview and ideas as to how these energy sources may be exploited in a more efficient way while minimizing the risk of the operations. It is now becoming clear to the public, local authorities, the geothermal industry and regulatory agencies that deep geothermal systems carry a small risk as do most technologies in the energy sector. Dams can break, nuclear power plants may fail, carbon dioxide released from oil and gas may contribute to global warming, and EGS projects may create damage through induced earthquakes. The open question is whether or not society is able to find ways to balance and accept and, most importantly, mitigate these risks. One aim of the present project is such mitigation as regards hydrocarbon and geothermal reservoirs. Fracture mechanics has become of great interest and importance in energy industries, both for geothermal and hydrocarbon energy sources. Fluid pumped under high pressure (or pressure generated underground with plasma) induces fractures, generating micro-earthquakes, thereby increasing the rock-body permeability and creating a reservoir for the fluid.

Hydraulic fracturing is one of the best techniques employed in oil and gas reservoirs to improve the turnover of production. In this phenomenon a highly pressurized fluid is pumped into a borehole resulting in creation of cracks which will be used to reach in stored resources in hard layers [Dong]. Primary models of hydraulic fracturing have assumed a neat crack evolving in a continuous medium [see Barani, shreffler,boone Spence mohammadnejad] which has been proved to be over idealized as nearly all reservoirs are full of faults affecting this phenomenon. Dahm has studied different reservoirs and has claimed the use of single crack models results in considerable error in estimations. The existence of faults – especially very large ones – could far change the crack propagation mechanisms; different behaviors of penetration, arrest, diversion and offset could be distinguished in case intersection takes place [Zhang 2007]. Multiple parameters will be important in final behavior of the intersecting cracks; fluid viscosity, angle between interfaces, crack lengths, friction coefficient and far field stresses. Hence general investigation of this event is a quite cumbersome task.

Hydraulic fracturing in medias with initial faults has been studied by different methods. A group of these research works are related to homogenous mediums.

Dong & Pater have represented a numerical implementation of displacement discontinuity method

2. NUMERICAL INTEGRATION

In finite element formulation shape functions and derivatives are polynomials. Dealing with polynomials, Gauss integration is best suited method as being optimum in accuracy and cost. In contrast for extended finite element the continuity is violated and functions are not smooth anymore. Hence new approaches have been proposed and employed to improve integration for such cases. Generally two methods are used in numerical simulations; Triangular partitioning and rectangular subgrids (see figure 1). In triangular partitioning the element area is divided into triangles aligned with the element edges and the interface. Performing integration over these triangles, integration functions will be smooth and consequently better approximation of integrals - even for singular functions1- will be given. On the other hand rectangular sub-grid method divides each element area into high number of rectangles distributed uniformly over the element. Although number of Gauss points required in this method is quite higher integration is less accurate in comparison with triangular partitioning, as integrands are non-smooth over a number of sub-grids. Yet this approach is easier to handle and still accurate enough as great number of simulators utilize this method. Greatest interest to this method is its ease of implantation in simulation and moreover superiorities in crack propagation process. It must be added while in triangular partitioning Gauss points alter during solution in same element – which results in data transfer from old Gauss points to new ones- in rectangular sub-girds Gausses are fixed. This would improve the performance of the simulation.

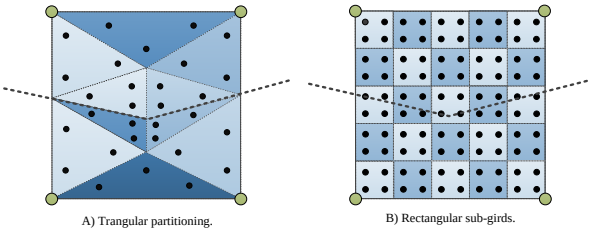

A) Trangular partitioning. B) Rectangular sub-girds.

Figure 1 different methods of integration for enriched elements

An important issue in integration is incompatible enrichment. Incompatible enrichment is a result of enriching an element with interface crossing too close to an edge or a node. Consequently integrated values for some enrichment functions (e.g. Heaviside) will be too small. This problem arises as normally values related to enriched DOFs are some orders of magnitude lower than the standard ones. Hence it will end in ill conditioning of stiffness matrix and other parameters involved and instability of solution or lack of convergence will be observed.

Incompatible enrichment is usually evaded by not enriching the element. In fact it is assumed the interface crosses exactly the close node. Although this will add a minor approximation to the solution however as the element size is very small - especially for crack problems - It would be negligible. The criterion for not enriching the element is usually the area ratio of smaller portion produced by the interface (A_1) to the total area of the element (A). This value is represented by R_A and it is usually set to 10^{-4} suggested by Dolbow. This method is more suited for triangular partitioning method. Another criterion suggested by Mohammadi is existence of a number of Gauss points (even a single one) in smaller portion. It is evident this method is applicable in rectangular sub-grid method for having a uniform distribution of Gauss points Figure 2.

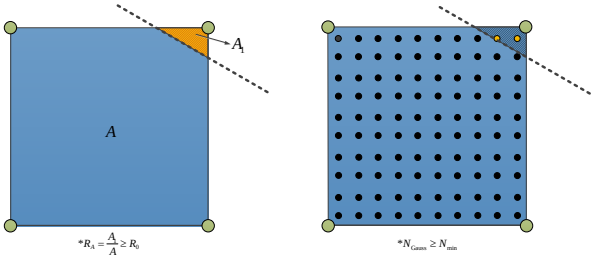

A) Area ratio method. B) Minimum Gauss points method.

Figure 2 Critical conditions for enriched elements.

3. CRACK GROWTH

As explained in previous sections, crack propagation is a cumbersome procedure finite element method. Remeshing and data transfer are costly and time consuming, resulting in lower performance. Moreover the need of a very fine and condense mesh around the crack tips in order to capture high stress gradients around would accent the problem. In contrast to the classic finite element, the extended one does not require any data transfer and remeshing where change of discritization would handle the interface evolution. Moreover the existence of higher order interpolation – especially at the crack tip - could eliminate the need of very fine meshes over these zones.

Although crack propagation process is handled gratefully in XFEM, some special provisions must be considered. The important point is despite in preliminary papers on XFEM change of discritization would be the only requisite for crack propagation, new developments represent some loss of accuracy for this approach - especially for dynamic cases. Rethore et al. has shown during crack propagation procedure the omission of old crack tip DOFs would result in loss of energy. Instead these DOFs must be hold and vanish gradually during the solution of next steps. This approach has been quite appropriate and successful as represented in the original paper, though as being

quite cumbersome to develop the algorithm and no benefits for quasi static cases it has not been utilized in the simulation.

An important factor in crack propagation modeling is the criterion utilized for determining the threshold and direction of crack evolution. Generally in LEFM stress intensity factor (SIF) is used for assessment of these parameters. The J -integral, introduced by Eshelby , is one the most precise methods in estimation of SIF which is defined as below,

$$J=\int_{\Gamma\cup\Gamma_{d+}\cup\Gamma_{d-}}(\frac{1}{2}\sigma_{ik}\varepsilon_{ik}\delta_{1j}-\sigma_{ij}u_{i.1})n_j\mathrm{d}\Gamma \qquad (35)$$

Where δ is Kroner delta operator, n_j is j -th component of unit normal vector to the closed contour and x_1 is the axis tangent to the crack at tip (see figure 1 (A)).

Based on Mohammadi J -integral could be calculated via different methods e.g. nodal solution, general finite element solution, equivalent domain integral and interaction integral. The interaction integral method is known as the most exact method among these methods and has been employed in the current study. According to this approach first the contour integral is rewritten in domain form, which is more suitable for finite element formulation. It follows,

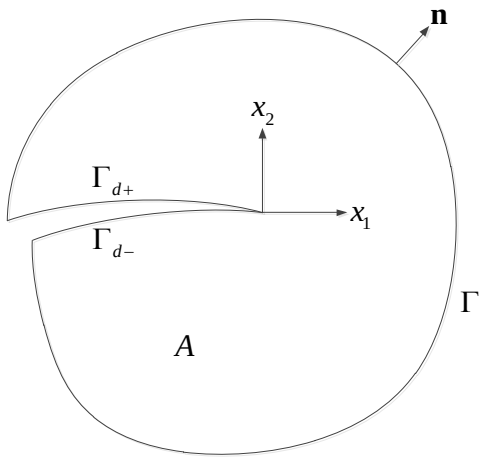

A) Nomenclature for *J*-integral.

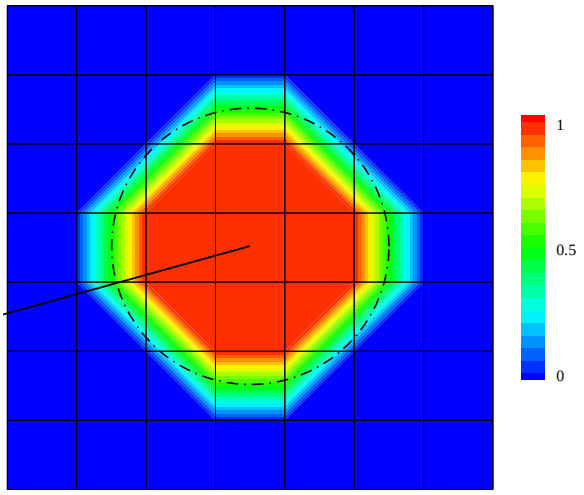

B) *q*-weight function.

Figure 3 (A) Contour for *J*-integral and parameters involved. (B) *q*-weight function with radius $R=2a$ (where a is average element size).

$$J=\int_A(\sigma_{ij}u_{i.1}-\frac{1}{2}\sigma_{ik}\varepsilon_{ik}\delta_{1j})q_{,j}\mathrm{d}\Omega+\int_{\Gamma_{d+}\cup\Gamma_{d-}}(\frac{1}{2}\sigma_{ik}\varepsilon_{ik}\delta_{1j}-\sigma_{ij}u_{i.1})qn_j\mathrm{d}\Gamma \qquad (36)$$

Next by employing an auxiliary field with known analytical solution (stated by superscript (2)) and employing superposition of this filed with the present field (stated by superscript (1)), it deduces,

$$J^{(1+2)}=J^{(1)}+J^{(2)}+I^{(1,2)} \qquad (37)$$

Where $I^{(1,2)}$ is the interaction integral defined as below,

$$I^{(1,2)}=\int_A(\sigma_{ij}^{(1)}u_{i.1}^{(2)}+\sigma_{ij}^{(2)}u_{i.1}^{(1)}-\frac{1}{2}\sigma_{ik}^{(1)}\varepsilon_{ik}^{(2)}\delta_{1j})q_{,j}\mathrm{d}\Omega+\int_{\Gamma_{d+}\cup\Gamma_{d-}}(\frac{1}{2}\sigma_{ik}^{(1)}\varepsilon_{ik}^{(2)}\delta_{1j}-\sigma_{ij}^{(1)}u_{i.1}^{(2)}-\sigma_{ij}^{(2)}u_{i.1}^{(1)})qn_j\mathrm{d}\Gamma \qquad (38)$$

And,

$$I^{(1,2)}=\frac{2}{E^*}(K_I^{(1)}K_I^{(2)}+K_{II}^{(1)}K_{II}^{(2)}) \qquad (38)$$

Where E^* equals E for plane stress and $E/(1-\nu^2)$ for plane strain. Wise choice of auxiliary fields is assuming pure mode I or pure mode II resulting in vanishing of $K_{II}^{(2)}$ or $K_I^{(2)}$ respectively.

It must be noted for traction free interfaces, which are quite common in mechanics, the second term in expression (38) vanishes. However as in this study the interfaces are pressurized this integral must be considered. Another note in that for the first term of expression (38) only gradient of q exists, hence this integral is performed over narrow band represented in figure 1(B). However for the second term q equals unity for the interior of this band. It must be added narrow band for the weight function q is used for example by Bordas and has been employed in here. There are other approaches where this function is assumed to be disk see for example Moes & Belytschko. It must be mentioned both methods are acceptable as been used extensively by different research works Figure 3.

Last note here will be on the use of SIF in crack growth. Different criterions has been introduced and used for crack propagation, yet the simplest and more common one is the fracture toughness K_{IC}. Whenever the K_I exceeds this value crack growth takes place. Moreover SIFs could be used to determine the crack propagation direction. A prevalent expression for crack growth direction is as below,

$$\theta = 2\arctan[\frac{1}{4}(\frac{K_I}{K_{II}} \pm \sqrt{(\frac{K_I}{K_{II}})^2 + 8})] \qquad (39)$$

Where this value is computed with respect to x_1. The crack would propagate a length equal to element size in each growth increment. It must be added in each propagation step, as multiple cracks are considered in here, crack intersection should be controlled. As only one set of enriched DOFs are considered in each element, if distance between two crack interfaces becomes lower than a single element the automatically intersects the interfaces. It is evident that crack tip enrichments are "killed" and are replaced with junction enrichment function. This algorithm is quite similar to algorithm proposed by Budyn et al. . Remember that in this study it is assumed only one crack could propagate and other cracks are considered as pre-existing faults. Else an energy analysis is required to determine which crack tip must propagate as explained in reference [Budyn].

4. NUMERICAL SIMULATION RESULTS

In this section five examples are chosen to investigate the validity of the proposed method. First example will study three cracks with varying distances under uniform tension. Second example will be a single crack with uniform internal pressure which a basic solution for HF where SIFs will be verified with available solutions. Last three problems will study the interaction phenomenon between HF and natural fault. Fourth and fifth examples are chosen to show HF crack is propagating in naturally fractured porous medium. This example will study mixed mode crack propagation. Fourth example is HF crack interacting with natural fault of existing fracture with different directions. This example Figure 4 will study mode I and mixed mode crack propagation. Final simulation is chosen so show what is going to happen after the interaction between HF crack and natural fault in the case of 90 degree angle existing fault in porous medium. Material properties for all five examples are Granite and they have been given in Table1.

Table 1: Properties of rock

50.2e9	Young Modulus
0.25	Poisson's Ratio
2700	Solid Density kg/m^3
1000	Fluid Density kg/m^3
0.21	Porosity %
0.2	Permeability mD

First example is three cracks with size of 0.5 meter in porous medium with tension of 1e10^{+6} Pa.

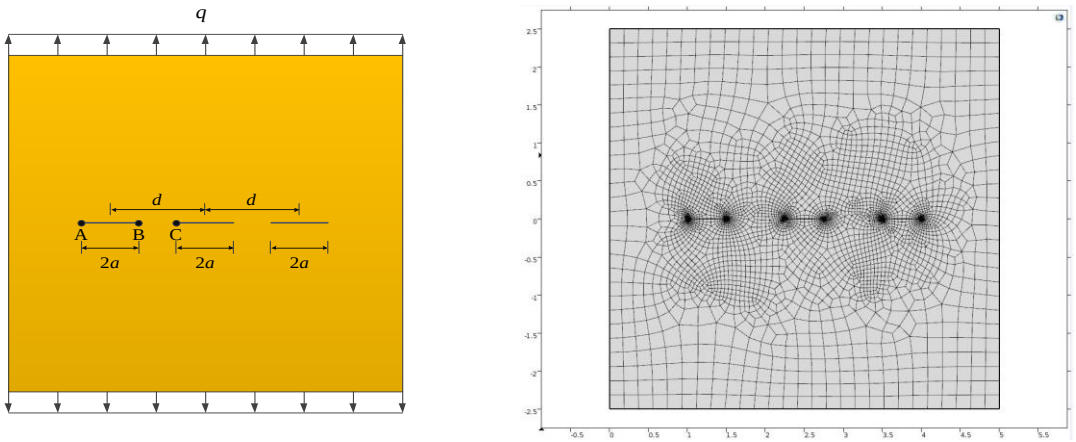

Figure 4. Three cracks with offset under uniform tension - problem's configuration.

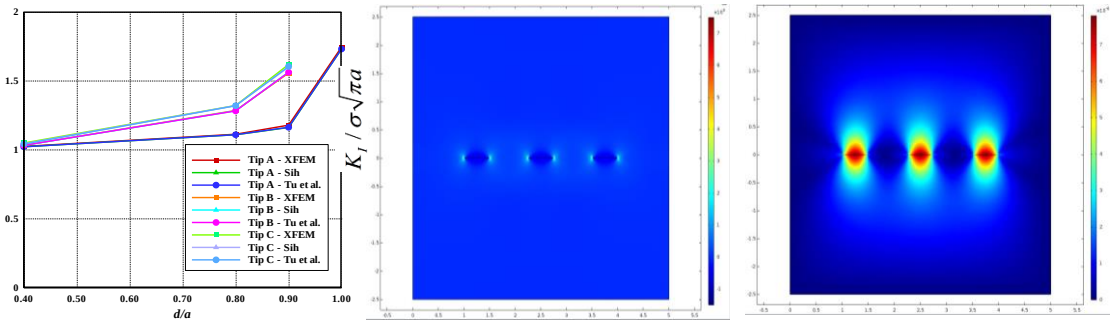

Figure 5. Stress Intensity Factor for plate with three cracks at tips A, B and C.

Again in this example plate of problem 1 is considered with the same material properties. Figure 6 plain strain condition is assumed. A crack of length 2 meters is positioned at the center of the plate and is subjected to a uniform internal pressure of $1e10^{+6}$ Pa.

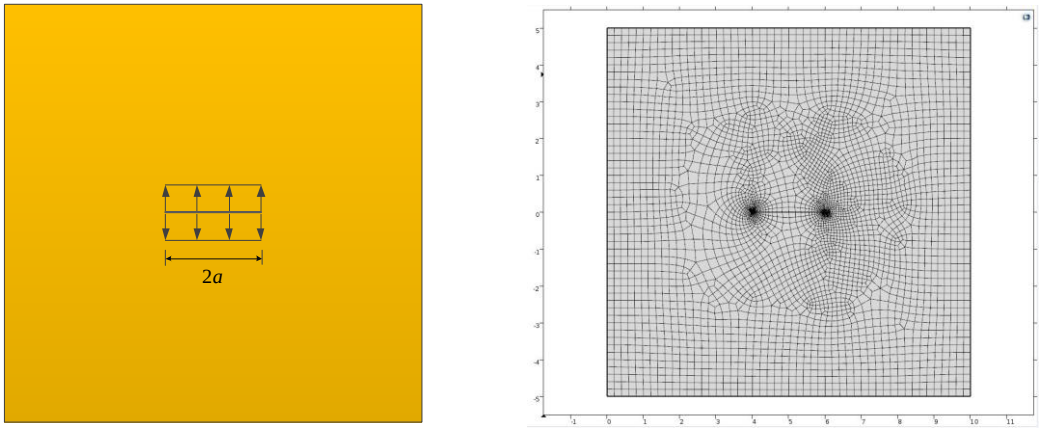

Figure 6. Single crack subjected to internal pressure – problem's configuration

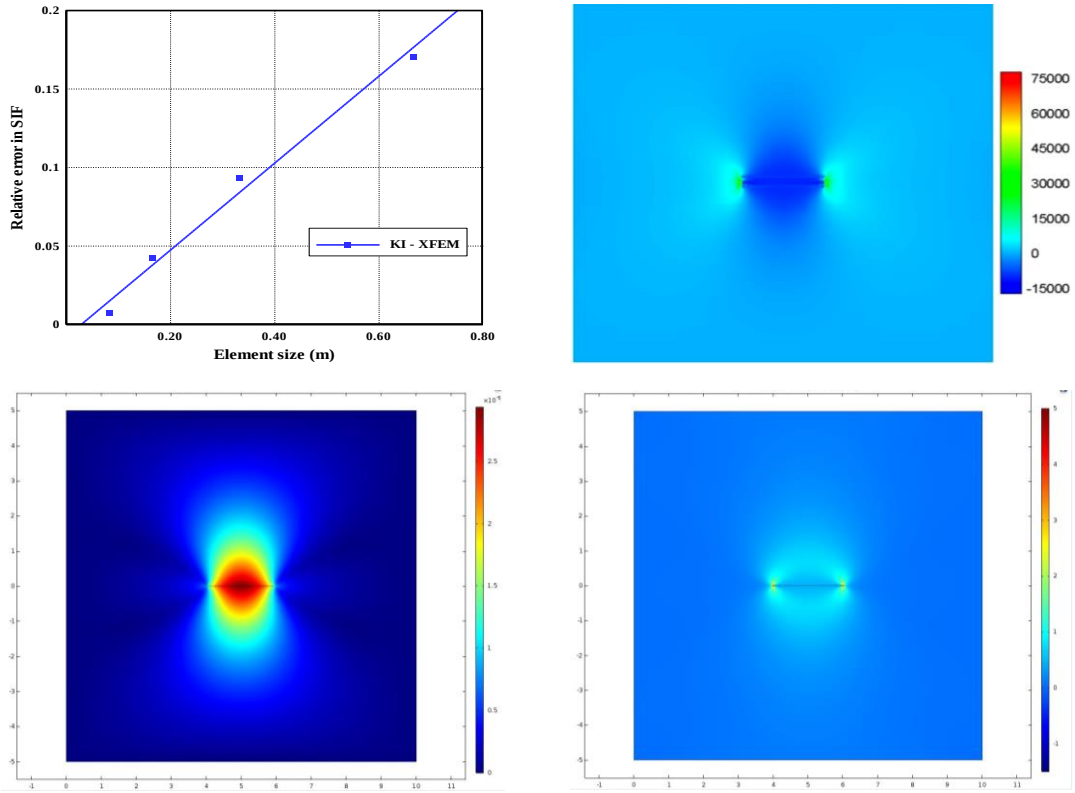

Figure 7. Principal stress and total displacement contours which shown stress concentration around the crack tip and how fracture will propagate.

A plate with a kinked crack subjected to uniform tension is studied in this example. The dimension of the crack is assumed to be $10\text{m}\times10\text{m}$ a structured mesh of 6000 quadratic elements with 6171 nodes is utilized. A distributed force q equal to $1\ \text{KN/m}$ is exerted along the upper and lower boundaries with traction free condition for the crack edges. Plane strain condition has been assumed. The crack is composed of two segments of lengths $a=0.5\text{m}$ with a varying wing b of length ratios $b/a=0.2,\ 0.4$ and 0.6. Length c is defined as the horizontal projection of interface and is calculated by $2c=a+b/\sqrt{2}$ which is used as the characteristic length of the crack interface. The angle between the two segments of the crack, β, is assumed to be 45^0. Actually the crack dimensions are small enough with respect to the plates' in order to model infinite domain condition. The configuration of the plate and the corresponding interface is represented in figure 8. This problem has been represented in Murakami's handbook [14] and It is also resolved by Dong et al. using the displacement discontinuity method. In figure 9, results from these researches are represented together with XFEM simulation in here. Note that values of SIF from other researchers are scaled as being demonstrated dimensionless. Apparently great agreement is observed between these solutions.

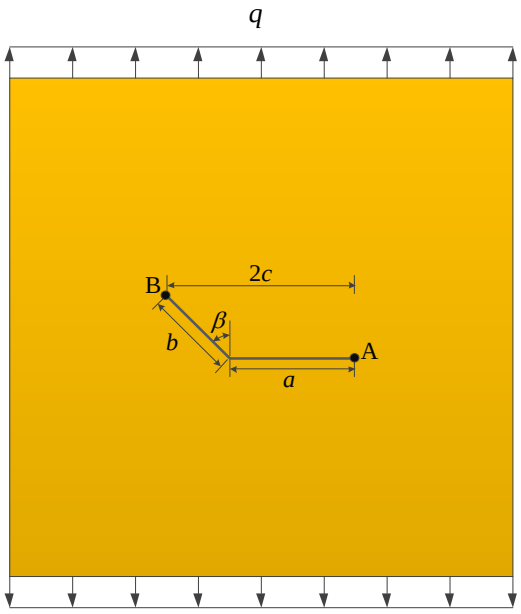

Figure 8 A kinked crack under uniform tension – problem's configuration.

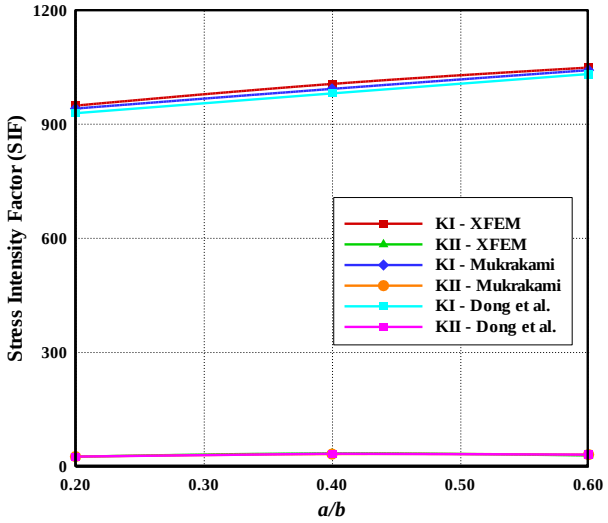

Tip A

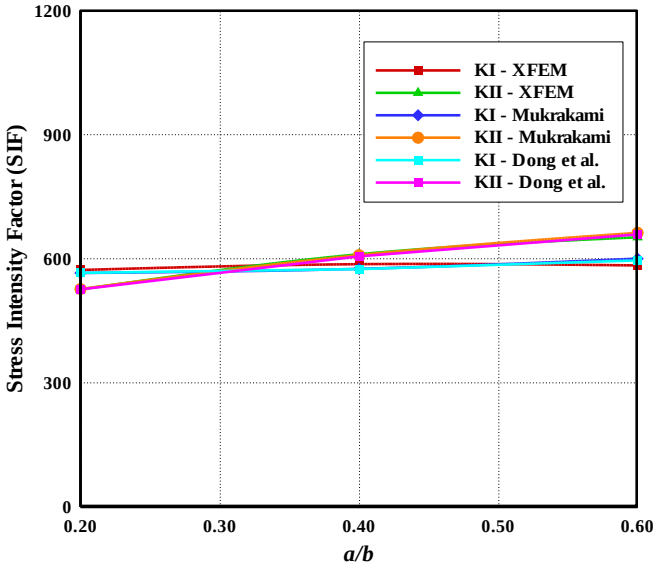

Tip B

Figure 9 Stress intensity factors (SIF) for tip A and B for plate with kinked crack.

Hydraulic fracturing arrest at a perpendicular fault A 2D domain is considered. The height of the domain H is 2200mm with width B equal to 1000mm. Suppose the domain is composed of a material plane strain condition is assumed for this example. A horizontal crack interface of varying length L_c is assumed which is subjected to uniform internal pressure of $p=1\text{MPa}$ along its whole length while a fault of length L_f equal to 2000mm is position vertically in the medium. This example does not study crack propagation, yet the length of L_i tends to zero in four steps, modeling shots of real crack propagation. Note that the length L_c+L_i equals 100mm where L_i's of $70\text{mm}, 40\text{mm}, 10\text{mm}$ and 0mm will be studied. The left crack tip (point A) is assumed fixed where B_l is equal to 400mm. Contact would happen during steps of solutions over some zones of the fault, where normal penalty springs

with stiffness of $K_N = 10^{10}$ MPa/mm will be emplaced where required. Note that in this example no frictional contact is supposed for the fault. A structured mesh of 3050 elements with 3162 nodes is assumed for the simulation. The configuration of this example with interfaces involved is represented in figure 10. Lots of problems have been designated in order to investigate interaction between hydraulic fracturing and natural faults [1,2,3]. This example has been chosen from Dyskin & Caballero. As mentioned, it is supposed that the fault is frictionless which according to this research it ends in arrestment of the hydraulic fracture. In figure 11 diagrams for implied cases is represented. Following results could be deduced from these diagrams which are in accordance with.

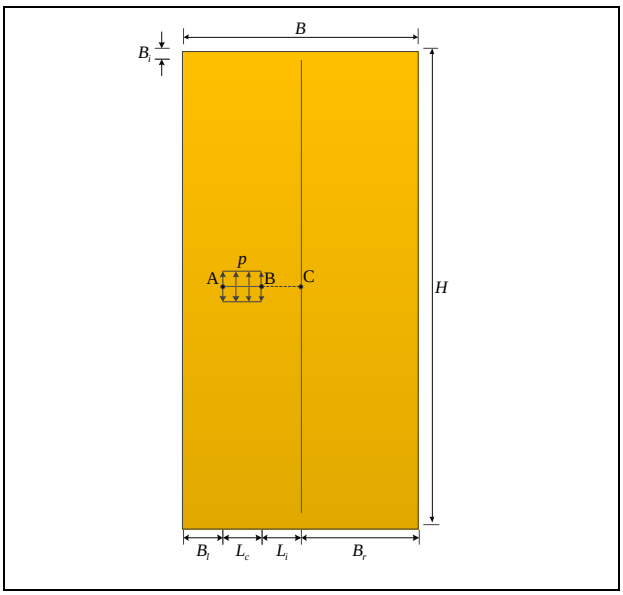

Figure 10 Hydraulic fracturing arrest at a perpendicular fault – problem's configuration.

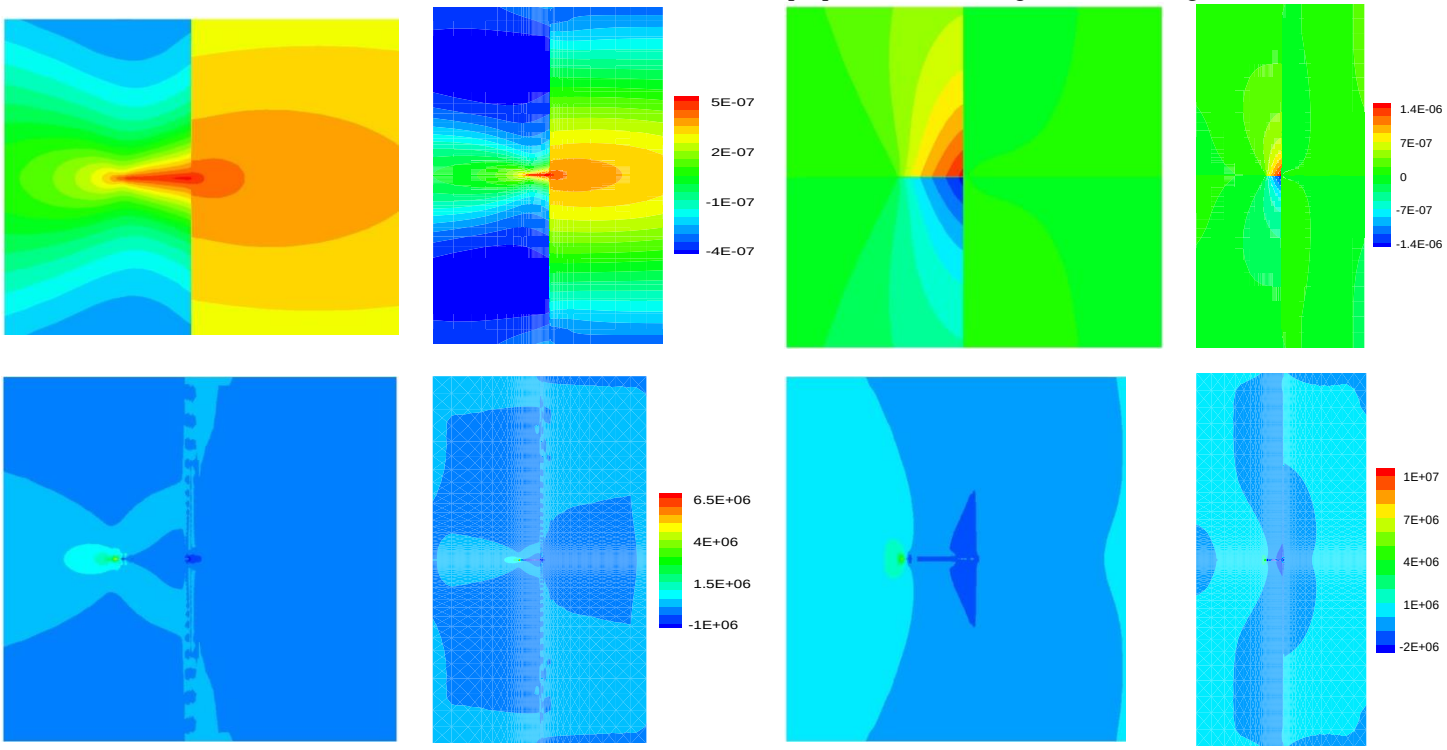

Figure 11 different contours for hydraulic fracturing arrest at a perpendicular fault for intersection condition ($L_i = 0$); A) Displacement in $x-$direction. B) Displacement in $y-$direction. C) Stress in $x-$direction. D) Stress in $y-$direction.

The opening of the fault could be categorized into two distinguished behaviors; before intersection and at the moment of intersection. While not intersecting, three zones could be distinguished: upper and lower flange opening; central opening and two zones of contact situated besides the central opening. As the interface evolves to the fault, the openings and contact tractions increases. But at the moment junction occurs the behavior alters instantaneously. Central opening vanishes and contact zone happens at the center of the fault. This is due to removal of the propagating crack tip which ends in omission of singularity in the stress field of the solution. An important factor in the arrestment of the interface is the stress filed just behind the fault. According to figure 11, as soon as the interface touches the fault, a compressive stress develops in $y-$direction at the point of junction. This means this point is not a candidate for crack propagation. Hence frictionless fault is a susceptible place for hydraulic fracture arrestment.

It must be added at the end of this example that contours for displacement and stress at the moment of

intersection are shown in figure 11. Implemented marks could be observed for this case especially the compressive stress developed behind the fault, resulting in crack arrestment. It should be mentioned all results from the simulation in here are in very good agreement with results from Dyskin et al., though Dyskin's study involves considerably finer meshing required for classic FEM solutions.

Next example is The sill in this section is transgressive and discordant i.e. Type 2 (Jackson, 2010) and feeds into faults to produce a vent which interacts with heterogeneous fluvial facies, coal and shallow marine shelf facies overburden Figure 12.

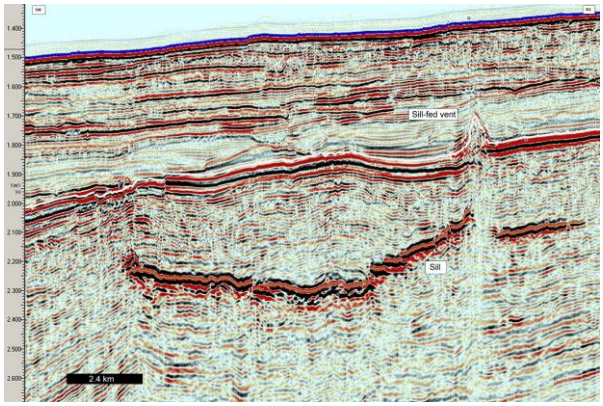

Figure 12: Is the raw seismic JPEG image to be numerically model (Jackson, 2010).

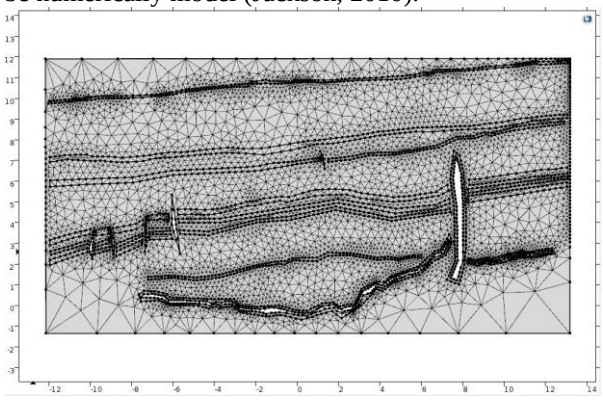

Figure 13: Is the numerical model with the empty cavities (faults, sill and vent modeled as a fault) taken from the difference.

Adding different boundary loads to either faults and/or sills at various magnitudes occurred to see different profiles. There are three main scenarios of boundary load, modelled in this project are in Faults and sills together. Loading is equal to the overburden pressure and tectonic forces. When sills are solid, they are stiff rocks and concentrate stress. When sills emplace in sedimentary rocks they are much stiffer than the host rocks and therefore concentrate stresses in the sedimentary layers close to where they emplace. This concentration of stresses corresponds to where the loading locates, on both tension and compression. In very shallow sections such as this seismic section, where the host rocks are still relatively soft, the sill will concentrate tensional stresses when the basin is undergoing extension Figure 13.

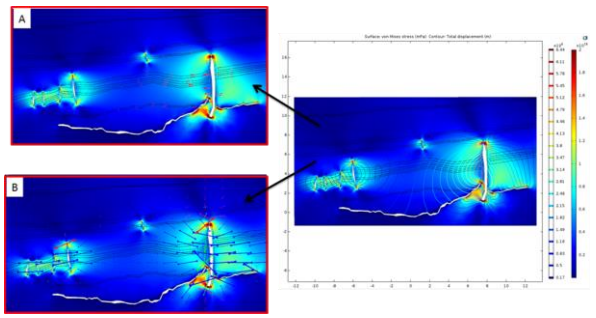

Figure 14: This is the SW faults and NE vent (fault) with a boundary load in all three diagrams (A, B and C) of 10MPa with different post processing inputs. Figure (A) shows the magnitude of the maximum compressive stress dying out over distance. Figure (B) shows the principle stress tensor directions with red arrows being the maximum compressive stresses located at the tips of the faults and vent orientated at a sub-horizontal position with the minimum compressive stress being mostly vertical. Figure (C) shows the compressive stress contours dying out the same as the stress arrows in (A) as we move away from the vent especially, (C) also shows how asymmetric the stress concentrations are around the section.

The study emphasized on consistency as the model was asymmetric due to the dip of the stratigraphy; asymmetric results were expected. With many analogue studies on sill interaction (Barnett and Gudmundsson, 2014) showing similar/analogous results there is significant evidence supporting the observations in this study.
Sills are primarily extension fractures and form perpendicular to the minimum principle compressive stress, for horizontal sills the emplacement is vertical, this does change locally where the sill tends to jump up a bed making it transgressive, which produces different directions of the minimum compressive stress to more horizontal much like a dyke at that time observed in this model Figure 14. The sill in this study emplaces along contacts within layered host rocks. On meeting a contact between layers, the sill is seen to respond in one of these three ways: arrested at the contact, penetrating the contact, or becoming deflected symmetrically or asymmetrically along the contact.

3. CONCLUSIONS

In the present paper, the hydraulic fracture propagation was presented in saturated porous media using the finite element method. We observe how it is going to propagate in intact medium or in naturally fractured medium as well. The main reason of risk and hazard control of this paper is all about HF cracks interactions with natural fault and ends up fault propagation. These fault propagations can easily flowing the HF fluid to the different area. Some of these badly oriented faults can ends up taking HF fluid to the underground water resources. This is highly unlikely but probable and we investigated it in this report.

To conclude the results have shed light on what we expect to see in a sedimentary basin that is under the emplacement of sills during hydrocarbon maturation processes and where the likely hydrocarbon accumulations can occur and where and for what circumstances stress accumulations and fault reactivation are likely to occur and for what reasons related to Sill emplacement. In addition, the results of this study suggest that numerical models need to model more complex host rock stratigraphy and rheologies if they are to capture the full range of deformation mechanisms that occur during sill emplacement in the Earth's shallow subsurface.

REFERENCES

Akulich AV, Zvyagin AV (2008) Interaction between hydraulic and natural fractures. Fluid Dyn 43: 428–435.

Barani OR, Khoei AR, Mofid M (2011) Modeling of cohesive crack growth in partially saturated porous media; A study on the permeability of cohesive fracture. Int J Fracture 167: 15-31.

J.N. Germanovich, A.V. Dyskin A model of brittle failure for material with cracks in uniaxial loading Mechanics of Solids, 23 (2) (1988), pp. 111–123.

L.N. Germanovich, A.V. Dyskin Fracture mechanisms and instability of openings in compression Int. J. Rock Mech. Min. Sci., 37 (1–2) (2000), pp. 263–284.

Dong CY, de Pater CJ (2001) Numerical implementation of displacement discontinuity method and its application in hydraulic fracturing. comput Methods appl Mech Engrg 191: 745-760

Lewis RW, Rahman NA (1999) Finite element modeling of multiphase immiscible flow in deforming porous media for subsurface systems. Comput Geotech 24: 41–63.

Lewis rw, schrefler ba (1998) the finite element method in the static and dynamic deformation and consolidation of porous media. Wiley, new york.

Zhang Z, Ghassemi A (2011) Simulation of hydraulic fracture propagation near a natural fracture using virtual multidimensional internal bonds. Int J Numer Anal Meth Geomech 35: 480–495.

A. Jackson, C., Magee, C. and Golenkov, B. (2013). Seismic Expression and Petroleum System Implications of Igneous Intrusions in Sedimentary Basins: Examples from Offshore Australia*. Search and Discovery Article, 10483.

Alden, A. (2016). See the Densities of the Most Common Rock Types. [online] About.com Education. Available at: http://geology.about.com/cs/rock_types/a/aarockspecgrav.htm [Accessed 1 Mar. 2016].

Barnett, Z. and Gudmundsson, A. (2014). Numerical modeling of dykes deflected into sills to form a magma chamber. Journal of Volcanology and Geothermal Research, 281, pp.1-11.

Community.dur.ac.uk. (2016). Foundations - Modulus of Elasticity. [online] Available at: http://community.dur.ac.uk/~des0www4/cal/dams/geol/mod.htm [Accessed 1 Mar. 2016].

Engineeringtoolbox.com. (2016). Dirt and Mud - Densities. [online] Available at: http://www.engineeringtoolbox.com/dirt-mud-densities-d_1727.html [Accessed 8 Mar. 2016].

Engineeringtoolbox.com. (2016). Poisson's ratio. [online] Available at: http://www.engineeringtoolbox.com/poissons-ratio-d_1224.html [Accessed 1 Mar. 2016].

Ged.rwth-aachen.de. (2016). Miri. [online] Available at: http://www.ged.rwth-aachen.de/Ww/projects/faults/Miri/Miri.html [Accessed 8 Mar. 2016].

Geotechdata.info. (2016). Soil elastic Young's modulus - Geotechdata.info. [online] Available at: http://www.geotechdata.info/parameter/soil-young's-modulus.html [Accessed 8 Mar. 2016].

Gudmundsson, A. and Lotveit, I. (2012). Sills as fractured hydrocarbon reservoirs: examples and models. Geological Society, London, Special Publications, 374(1), pp.251-271.

Jackson, C. (2010). VSA - Entity Details. [online] Seismicatlas.org. Available at: http://www.seismicatlas.org/entity?id=95677822-3c77-4407-b23f-6daf7cd961ab [Accessed 23 Feb. 2016].

Jackson, C., Schofield, N. and Golenkov, B. (2013). Geometry and controls on the development of igneous sill-related forced folds: A 2-D seismic reflection case study from offshore southern Australia. Geological Society of America Bulletin, 125(11-12), pp.1874-1890.

Miller, D., Plumb, R. and Boitnott, G. (2013). Compressive strength and elastic properties of a transversely isotropic calcareous mudstone. Geophysical Prospecting, 61(2), pp.315-328.

Pan, J., Meng, Z., Hou, Q., Ju, Y. and Cao, Y. (2013). Coal strength and Young's modulus related to coal rank, compressional velocity and material composition. Journal of Structural Geology, 54, pp.129-135.

Qiuliang, Y. (2016). Acoustic properties of coal from lab measurement. SEG Las Vegas 2008 Annual Meeting. [online] Available at: http://rpl.uh.edu/papers/PAPR525_Qiuliang.pdf [Accessed 29 Feb. 2016].

Spence, G., Redfern, J., Aguilera, R., Bevan, T., Cosgrove, J., Couples, G. and Daniel, J. (n.d.). Advances in the study of fractured reservoirs.

Szabo, T. (1981). A representative poisson's ratio for coal. International Journal of Rock Mechanics and Mining Sciences & Geomechanics Abstracts, 18(6), pp.531-533.

Acknowledgements

The Author is sincerely thanking IGA for their research grant support. And also Weld On Sweden company for their contribution.